Reduction of Static Electricity Meter Errors by Broadband Compensation of Voltage and Current Channel Differences

Zander Marais, Helko E. van den Brom, *Senior Member, IEEE,* Gertjan Kok, and Marijn G. A. van Veghel

***Abstract*— To compensate for the different transfer functions of the current and voltage input stages of static electricity meters, usually, a time correction is applied, which is suitable for sinusoidal signals. However, for highly distorted signals, in which the high-frequency content is significant, this method is insufficient and reading errors will not be fully compensated. For such waveforms, this article describes two alternative methods to deal with the different input stages. The methods are implemented on a home-built waveform recorder, modified as static electricity meter, and validated using their influence on energy-reading errors for various waveforms and input stages (impedance and coupling). Apart from highly distorted current signals, also the effect of finite source impedance is considered by modifying the voltage waveform accordingly, which potentially influences the observed meter errors as well. The inverse-filtering method is the most powerful method but is computationally intensive and, therefore, more suitable for high-accuracy power meters than for inexpensive electricity meters. The less computationally intensive equivalent-filtering method shows very good results as well and is a better candidate to be implemented in electricity meters. The latter is especially relevant because of recent results, showing that some electricity meters are sensitive to specific disturbances beyond the present standard test waveforms.**

***Index Terms*— Energy measurement, electromagnetic compatibility, electromagnetic interference (EMI), immunity testing, measurement errors, standards, watthour meters.**

I. Introduction

TESTING of electricity meters for billing purposes in the presence of disturbances mimicking realistic load conditions is crucial for customer confidence. Therefore, researchers and standardization organizations are investing in keeping up-to-date regarding common disturbances and related testing protocols [1]–[6]. Nevertheless, in the recent past, some static electricity meters that passed all relevant tests have been shown to be sensitive to specific conducted electromagnetic interference (EMI) [7], [8].

Though the metering errors are influenced by the specific load conditions [9], in order to eliminate them, their root cause should be investigated. Several mechanisms might introduce metering errors, such as the input impedance of the meter, saturation of magnetic cores, overloading of active input stages, or digital signal-processing techniques. These error mechanisms might be due to the specific choice of components or to more fundamental issues.

One of these fundamental issues is the phase mismatch between the current $I(t)$ and voltage $V(t)$, measured as a function of time t, due to different filtering mechanisms in the current and voltage probes. These filtering mechanisms introduce modifications of the waveforms that result in errors when calculating the instantaneous power $P(t) = V(t) \cdot I(t)$, leading to errors in the energy indication

$$E(T) = \int_0^T V(t) \cdot I(t) dt \tag{1}$$

calculated over a time period T by static electricity meters.

Manufacturers of energy calculation or power meter digitizer units are aware of this problem and implemented a correction method, aligning the instantaneous voltage and current samples by introducing a fixed phase shift, expressed in microseconds or in degrees, at the mains frequency of 50 or 60 Hz [10]–[13]. This time-shift method works perfectly fine for purely sinusoidal signals. However, in real-world low-voltage grids, both current and voltage waveforms show considerable distortions, whereas the voltage distortions in public electricity grids are usually within reasonable margins, as defined, for instance, in the EN 50160 [14], and the current and voltage waveforms that are induced by variable and nonlinear loads can show significant frequency components up to around 150 kHz and beyond [4], [7], [8].

A time-domain filtering algorithm for postprocessing instantaneous phase voltage and current samples to suppress detrimental dc offsets in the output signals of the voltage and current sensors is described in [15]. However, before using this algorithm to calculate active and reactive energies, the user first needs to implement a phase shift correction, for which it is suggested to introduce a time shift or, alternatively, to simulate the current-sensor high-pass filters and to propagate the phase voltage samples through the same filters [15].

In this article, we introduce and compare two methods to correct for the filter-response difference of the input stages to avoid errors in the calculation of energy in electricity meters. One of these methods is based on the equivalent-filtering suggestion in [15] and implemented real time, whereas the other is new and only used for postprocessing. The methods

Manuscript received July 7, 2020; revised October 20, 2020; accepted November 8, 2020. Date of publication November 20, 2020; date of current version December 18, 2020. This work was supported in part by the EMPIR Initiative co-funded by the European Union's Horizon 2020 Research and Innovation Programme, in part by the EMPIR Participating States, and in part by the Dutch Ministry of Economic Affairs and Climate Policy. The Associate Editor coordinating the review process was Yasutaka Amagai. *(Corresponding author: Helko E. van den Brom.)*

The authors are with VSL B.V., 2600AR Delft, The Netherlands (e-mail: hvdbrom@vsl.nl).

Digital Object Identifier 10.1109/TIM.2020.3039631

are compared in terms of their influence on properly time aligning the current and voltage waveforms as well as their influence on energy-calculation results. To do so, a home-built waveform recorder has been modified to function as an electricity meter. The goal, using the suggested broadband-compensation methods, is to achieve an accuracy of 2.0% for the highly distorted waveforms recorded using real physical loads that are known to cause metering errors in some static electricity meters and some further artificial signals inspired by these loads. Validation measurements of the energy readout of the home-built electricity meter with different filtering techniques have been performed using an earlier developed reference testbed [16].

II. Description of the Problem

A. General Description

When measuring distorted waveforms present in real low-voltage grids, the voltage and current signals are recorded using specific sensors having different transfer characteristics. The voltage signal needs to be scaled down from the mains voltage (typically 230 V in Europe) to lower values that can be measured by a digitizer, which can be done using a voltage transformer or a resistive divider that typically behaves as a bandpass or low-pass filter, respectively. Current signals are usually transferred into voltage signals using current transducers, such as resistive current shunts, Hall-effect current sensors, current transformers, or Rogowski coils. While current shunts and Hall probes typically behave as low-pass filters, current transformers have a passband and Rogowski coils behave as high-pass filters.

The standard solution to compensate for the difference in input stages is to introduce a time shift between voltage and current. Because a time shift is equivalent to a phase angle proportional to frequency, this solution is only suitable for pure sinewaves consisting of a single frequency, such as the mains frequency. However, for waveforms with a rich spectral content in both voltage and current such as highly distorted broadband waveforms caused by nonlinear loads, such as dimmed LED lamps [7], [8], other consumer electronics [17], [18], or renewable energy sources [19], this solution results in miscalculations and, consequently, reading errors.

B. Example: Rogowski Coil Current Sensor

To illustrate the consequences of incorrect compensation of filtering, consider a current waveform in which the power per cycle is concentrated in one positive and one negative very short pulse being measured with a Rogowski coil. When drawing such highly distorted current from the local low-voltage grid, the voltage will be distorted as well, depending on the grid impedance. For the correct calculation of the instantaneous power and accumulated energy, the positions of the current pulse and the distortion of the voltage (or even the instantaneous voltage for an undistorted waveform) should be properly aligned in time.

The operating principle of a Rogowski coil, typically consisting of an air-core coil, makes its linear within a high-current dynamic range with a typical bandwidth in the MHz regime. The output signal is proportional to the rate of change of the input current, i.e., the derivative dI/dt of the input current I with time t. Therefore, an integrator and a resistor are needed to convert the output signal into a voltage that is directly proportional to the input current. A high-pass filter is implemented to prevent overflow of the integrator in case of dc offset of the input signal.

This high-pass filter introduces a frequency-dependent phase shift, starting from 90° (for a first-order filter) at dc, decreasing and converging to zero with increasing frequency. Typically, at mains frequencies, the phase shift is on the order of 1°, whereas the high-frequency components will hardly be affected at all. Consequently, when introducing a time delay that is suitable for a 50 Hz or 60 Hz sinewave, the high-frequency components of the current pulse will be erroneously shifted in time. For instance, a time shift corresponding to 1° at 50 Hz would result in 40° at 2 kHz and 200° at 10 kHz. Therefore, the current pulse and the voltage signal will be misaligned, which can cause significant errors in the energy calculation of distorted waveforms.

III. Experimental Demonstration of the Problem

A. Experimental Setup

Waveforms as described in Section II can be investigated experimentally showing the phase-mismatch problem when using voltage and current sensors with different filtering characteristics. For the experiments described in this article, single-phase voltage and current signals are generated using a reference testbed designed for testing of electricity meters under distorted load conditions [16]. The reference testbed has a bandwidth of approximately 150 kHz and is able to measure the waveforms with an uncertainty of less than 0.10% with a 95% confidence level (or 0.05% standard uncertainty). The generated signals are then applied to a home-built waveform-capturing device that has been modified to function as a static electricity meter.

This home-built electricity meter uses an eight-channel 16-bit digitizer unit with 1 MHz sampling rate, suitable for performing three-phase voltage and current measurements. Digitizer channels can be either dc or ac coupled, where ac coupling is performed by introducing a series capacitance of around 160 nF, introducing a high-pass filter with a lower cutoff frequency of about 1 Hz for low-impedance voltage sources. An onboard computer with dedicated software is used to process the measurement data, apply filtering techniques to calculate the active energy, and store the corresponding voltage and current waveforms. Gain settings of the different channels are calibrated and corrected using the reference testbed.

The home-built electricity meter is designed for an accuracy of 0.5% for sinusoidal signals at 50 Hz, and the target is to reach an accuracy of 2.0% for highly distorted waveforms that are known to cause metering errors in some static electricity meters. The electricity meter has an optical pulse output, which generates 1000 pulses per kWh. The testbed determines the time between two or more pulses to calculate the corresponding energy. The duration of each test is chosen such that enough pulses are registered for a stable and reproducible

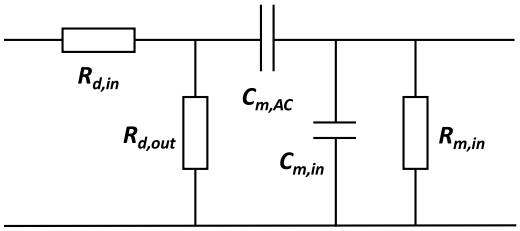

Fig. 1. Schematic of the voltage divider and input stage of the digitizer. $R_{d,\mathrm{in}}$ and $R_{d,\mathrm{out}}$ are the divider input and output resistance, $R_{m,\mathrm{in}}$ and $C_{m,\mathrm{in}}$ are the meter input resistance and capacitance, and $C_{m,\mathrm{ac}}$ is the ac-coupling capacitance that is shorted in dc-coupling mode.

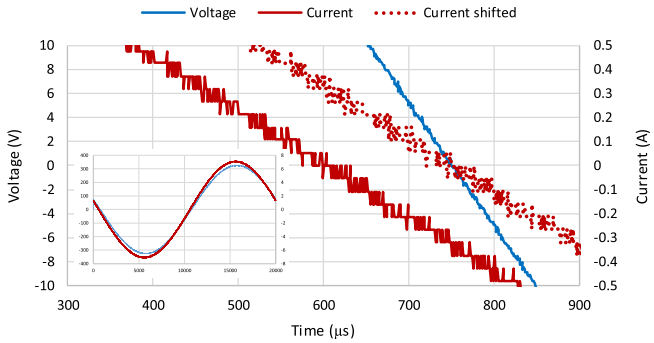

Fig. 2. Effect of different input stages on a sinusoidal 50 Hz, 230 V, 5 A waveform with power factor PF = 1, measured using the 16.8M-R divider and Rogowski coil (solid line) with the digitizer ac coupled. When applying a time shift of 150 μs to the current waveform (dotted line), the zero crossing of current and voltage coincides. Inset: same figure with expanded axes to show a full cycle of the uncorrected waveforms.

result, which is typically between three and ten pulses depending on the active power of the applied signal.

Voltage measurements are performed using three different resistive voltage dividers connected to the input of the digitizer, as schematically shown in Fig. 1. The first divider, referred to as 16.8M-R, is just a series resistor of 16.8 MΩ that effectively behaves like a voltage divider when used in combination with the 1 MΩ input resistor of the meter. The second divider, referred to as 16.8M-RC, is the same as the first, but to compensate for the cable capacitance and the input capacitance of the digitizer, the resistor is shunted with a parallel capacitor (not shown in the figure) to increase the bandwidth. The third divider, referred to as 1.68M-RC, consists of an input resistor of 1.68 MΩ and an output resistor of 100 kΩ that shunts the 1 MΩ input resistance of the digitizer, whereas the input and output resistors are shunted with a parallel capacitor to increase the bandwidth as well. In this way, we can investigate the influence of the bandwidth of the voltage divider as well as the input impedance on the performance of the compensation methods and emphasize the differences.

When using the digitizer in ac-coupling mode, the impedance of the corresponding coupling capacitor of around 160 nF is dominated by the divider high-ohmic input resistance for the lower frequencies. Consequently, for these high input resistors, the digitizer input is effectively dc-coupled.

The current is measured using a Rogowski coil with a high-pass lower cutoff frequency of 0.3 Hz and a bandwidth of 1 MHz. The Rogowski coil is suitable for recording current variations as fast as 30 A/μs.

B. Sinusoidal Signals

When measuring purely sinusoidal voltage and current waveforms using the 16.8-MΩ input resistance divider and the Rogowski coil with ac coupling for both channels, Fig. 2 shows that the resulting relative phase shift is equal to 0.15 ms or 2.7° at 50 Hz. It should be mentioned that the current and voltage signals have been corrected for dc offsets and that the initial phase of the waveform is arbitrary since no trigger event is used. When calculating the energy consumption or the average power for an integer number of cycles, this corresponds to an error of 0.11% for sinusoidal voltage and current signals that are fully in phase, i.e., power factor PF = 1, where PF is defined as the ratio between active power and apparent power, which is equal to the cosine of the phase angle between voltage and current for sinusoidal signals. This might still be acceptable, but the error value increases to 2.9% for PF = 0.8. For sinewaves, this error can be compensated by introducing a mathematical time shift of, in this case, 0.15 ms to the relevant measurement channel before calculating the power and energy, as mentioned in Section I and used in [10]–[13].

It should be noted that when the digitizer channels are dc-coupled, the phase shift is only 0.4°, which is mainly caused by the Rogowski coil as confirmed by separate verification measurements. The reason for the much larger difference in ac-coupling mode is the resistive divider influencing the input stage of the digitizer such that it is effectively dc-coupled, as discussed at the end of Section III-A. For dc coupling, with a phase shift of 0.4°, the resulting power or energy error values are 0.002% for PF = 1 and 0.42% for PF = 0.8, whereas the corresponding time shift is 22 μs.

C. Nonsinusoidal Signals

To illustrate the effect of a correction of the phase displacement due to the different filters using a time shift for nonsinusoidal signals, a highly distorted current waveform as caused by a series of compact fluorescent lamps and LED lamps in combination with a phase-fired dimmer is measured [7], [8]. For a dimmer setting of 75%, the energy of the current waveform is highly concentrated in one large current pulse (with peak value above 50 A and a maximum rate of change dI/dt higher than 2 A/μs) for each half cycle, which is strongly delayed with respect to the maximum of the voltage waveform [17] (see the inset of Fig. 3). Due to the finite grid impedance, the voltage waveform is distorted as well, showing a sharp dip simultaneously with the current pulse. These voltage and current waveforms are referred to as CL75.

Measurements of the CL75 current and voltage waveform with and without time-shift correction are shown in Fig. 3. As can be observed, without correction, the onsets of the current and voltage disturbances are very well synchronized. The time shift of 0.15 ms introduced to correct for the

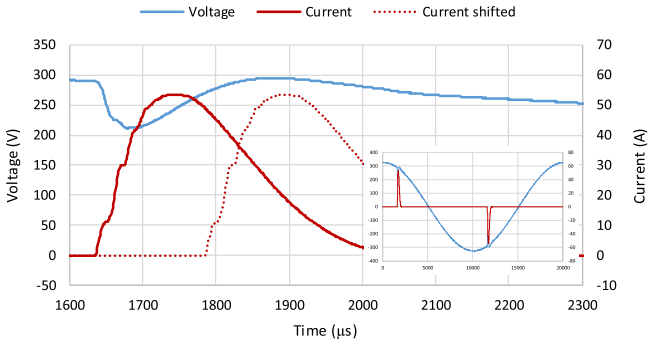

Fig. 3. Effect of the time shift on CL75 voltage and current waveforms. The measurements are performed using the same system and settings as in Fig. 2 (solid lines). The 150 μs time shift necessary to synchronize the sinusoidal current and voltage waveforms now introduces a phase mismatch for the high-frequency distortions (dotted line). Inset: same figure with expanded axes to show a full cycle of the uncorrected waveforms.

phase mismatch of the 50 Hz sinusoidal voltage and current waveforms of Fig. 2, however, it now introduces a timing error between the current pulse and the resulting voltage distortion. This is in line with the explanation in terms of the misalignment of higher frequency components given at the end of Section II-B.

The error introduced by the time shift Δt can be calculated from the time integral of the product of the voltage signal and the time-shifted current signal, $E(T) = \int_0^T V(t) \cdot I(t + \Delta t)dt$. When doing so for the original and time-shifted signals shown in Fig. 3, the energy reading for the latter would be 10.5% too high. The reason is that instead of multiplying the high current values with the distorted lower voltage, it is multiplied by the higher voltage occurring 0.15 ms later.

IV. Improved Compensation Methods

A. General Approach of the Improved Methods

As an alternative to introducing a time shift suitable for a single-frequency waveform only, a frequency-dependent phase shift should be applied. A frequency-dependent phase shift can be implemented mathematically in software. In this article, we describe two of such improved phase-mismatch compensation methods. The first method consists of the implementation of inverse filters to correct for the filtering behavior of the voltage and current sensors. The second method ensures that the voltage and current signals effectively propagate through equivalent filters such that the instantaneous measurement values are properly multiplied over the whole frequency range, as suggested in [15]. Both methods have their pros and cons and will be demonstrated on experimental data.

B. Inverse-Filtering Method

The first alternative method is to implement an inverse filter for both input stages such that the modified measurement data better represent the real voltage and current signals that are applied to the respective sensors. The basic idea here is to measure the complex transfer function of all components involved, multiply the Fourier transform of current and voltage signals by the inverse transfer function, and calculate the inverse Fourier transform of the result.

More formally, the inverse-filter method can be described as follows. Let $V_0(t)$ be the measured voltage signal in the time domain and $V_0(f)$ its representation (as complex-valued function) in the frequency domain. Let $r_V(f)$ be the gain correction factor of the voltage channel of the digitizer at frequency f and $p_V(f)$ the phase error at frequency f of the channel. Let $P(z)$ denote the phase of the complex number z and $|z|$ its amplitude. The corrected voltage signal in the frequency domain $V_1(f)$ now follows from:

$$V_1(f) = \frac{|V_0(f)|}{r_V(f)} e^{i[P(V_0(f)) p_V(f)]}. \tag{2}$$

The inverse Fourier transform of (2) yields the corrected voltage signal $V_1(t)$ in the time domain. Similarly, the measured current signal $I_0(t)$ can be corrected based on the gain correction factor $r_I(f)$ and the phase error $p_I(f)$ of the current measurement channel yielding a corrected signal $I_1(t)$. The corrected energy can then be calculated as $E_1(T) = \int_0^T V_1(t) \cdot I_1(t)dt$. Note that, in practice, the voltage and current are measured at discrete times t_i. The discrete Fourier transform is applied, and the correction is done at discrete frequencies f_i.

The transfer functions of the Rogowski coil, resistive divider, and digitizer ac-coupling mechanism used in the home-built waveform recorder were measured as follows. Using a calibrator, a sinusoidal signal of varying frequency was generated and applied to multiple channels of the digitizer of the home-built electricity meter. One of these channels is connected in the dc-coupling mode without transducer and used as a reference. The voltage dividers are connected to the remaining channels and the ratio and phase errors calculated through comparison with the reference channel. For the Rogowski coil, the generated voltage was converted into current using a high-precision transconductance amplifier. This current was applied to the Rogowski coil and a reference broadband current shunt having negligible phase and magnitude correction up to at least 100 kHz [20]. The ratio and phase errors of the Rogowski coil were then calculated by comparing the output voltages of the two current transducers using the same digitizer. The frequency of the applied signal was increased in quasi-logarithmic steps to cover the range between 10 Hz and 150 kHz. For frequencies in between measurement points, linear interpolation was used to estimate the magnitude and phase values. Measurements of the voltage dividers and Rogowski coil were performed with ac and with dc coupling.

The transfer functions obtained this way for the voltage dividers and the Rogowski coil are shown in Fig. 4. For the sake of comparing the transfer functions, the vertical scales are the same for all graphs. For the 16.8M-R divider that has no parallel capacitor, the bandwidth is only a few kilohertz, whereas the 16.8M-RC and 1.68M-RC dividers are much more broadband. The most relevant difference between the latter two is the phase displacement at lower frequencies, which is significantly larger for the 1.68M-RC divider when using the digitizer in ac-coupling mode, comparable to the Rogowski

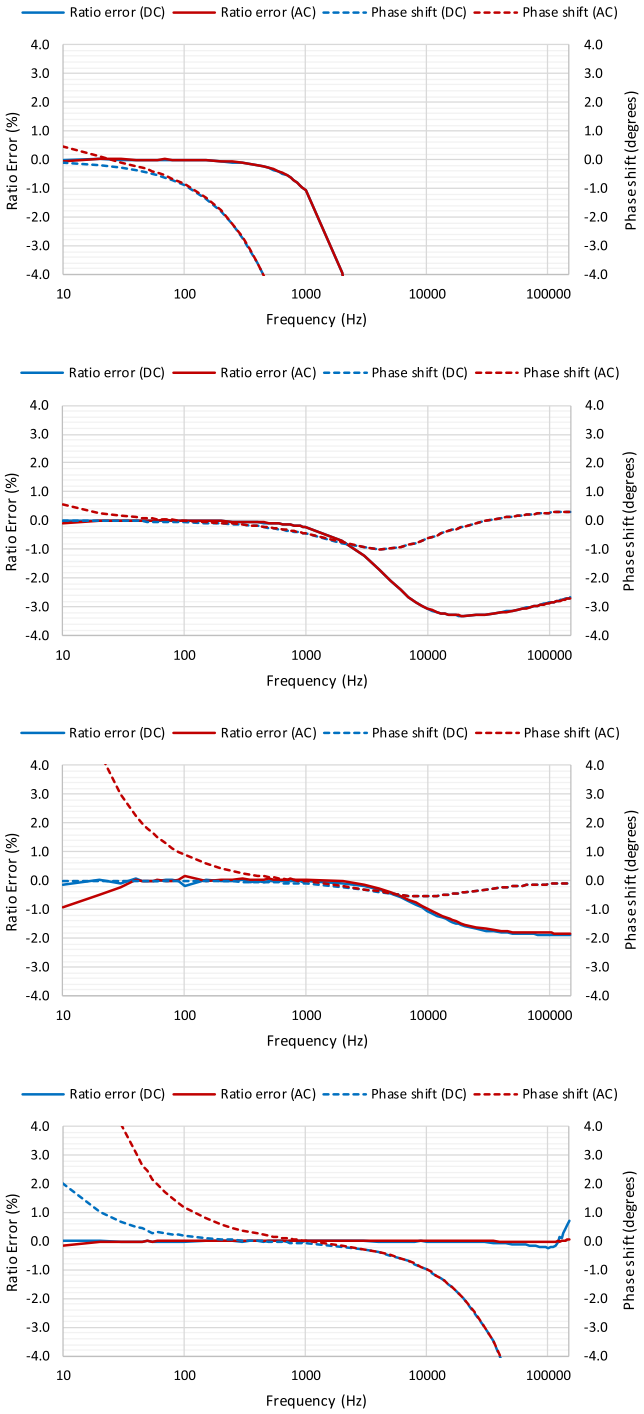

Fig. 4. Top to bottom: measurement results for the transfer functions of the resistive voltage dividers 16.8M-R, 16.8M-RC, and 1.68M-RC, respectively, and the Rogowski coil, for magnitude and phase.

coil. Hence, when the digitizer is used in the ac-coupling mode for both voltage and current, the 16.8M-RC and 16.8M-R dividers will behave almost as if they are dc-coupled. The reason for this is the high input resistance of the 16.8M-RC that dominates the digitizer ac-coupling capacitor for the lower frequencies, as explained in Section III-A. This will be significant already at 50 Hz where a phase difference of a few degrees between the voltage and current channels will have an impact on the energy readings, as demonstrated in Section III-B.

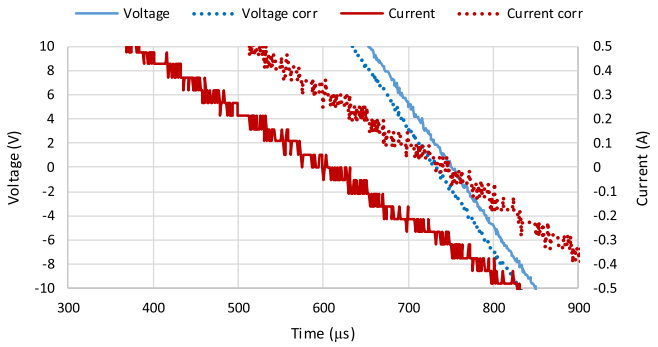

Fig. 5. Effect of the inverse-filter correction on a sinusoidal 50 Hz, 230 V, 5 A waveform with power factor PF = 1 (zoomed to the zero crossing). The measurements are performed using the same system and settings as in Fig. 2. Very good synchronization is obtained for the voltage and current waveforms after the inverse-filter correction (dotted lines). For the CL75 waveform, the inverse-filter correction has no visible influence (not shown in the figure).

When determining the inverse transfer functions of the Rogowski coil and voltage dividers, it should be noted that at high frequencies, the magnitude correction for the low-bandwidth voltage divider 16.8M-R is rather high. Consequently, when implementing the full inverse function, the high-frequency noise will be amplified. To reduce the noise level, the inverse transfer function was slightly modified; since it was shown in Section III-C that the onsets of high-frequency current and voltage disturbances are very well synchronized without correction already, the magnitude corrections at 20 kHz and higher were set to unity. Above 150 kHz, no correction is performed at all, i.e., the phase correction is set to zero. The amplitude correction factors between 10 Hz and 20 kHz are between 1.0 and 3.1 and the phase corrections lie between 0.5° and –85°, and therefore, no numerical instabilities are expected using this procedure.

To implement the inverse-filter correction method, the direct Fourier transform of the measurement data is multiplied by the modified inverse transfer function. Using the generalized version of Parseval's theorem, the energy can be calculated in the frequency domain from these corrected Fourier transforms [21]. For illustrative purposes, Fig. 5 shows the inverse direct Fourier transform of the corrected Fourier transform for the same measurement of a sinusoidal 50 Hz, 230 V, 5 A waveform with power factor PF = 1, as shown in Fig. 2. As expected, the originally observed 0.15 ms mismatch introduced by the different input stages is now properly corrected to within a few microseconds. When zooming in to the abrupt current and voltage distortions for the CL75 signal as presented in Fig. 3, the data corrected using the inverse filter showed no visible changes with respect to the original distortions (not shown in the figure), which were very well synchronized without correction already.

This method was not directly implemented in the data-acquisition software for real-time correction because Fourier transforms are rather computationally intensive. Other techniques might be used to reduce the computation time, but for this article, the corrected waveforms and the corresponding energy were calculated afterward based on ten cycles of the recorded uncorrected waveforms instead.

C. Equivalent-Filtering Method

The second method aims to ensure that the voltage and current channels are exposed to equivalent filtering characteristics at their input, in contrast to the first method where an inverse operation is applied. Because of the highly different nature of voltage and current sensors, the idea is to implement a software filter mimicking the voltage-channel characteristics in the current channel and vice versa.

As can be seen in Fig. 4, in the dc-coupling mode, the voltage dividers show negligible magnitude and phase errors at low frequencies. The input stage of the Rogowski coil in the dc-coupling mode can be represented by a high-pass filter with the cutoff frequency of 0.3 Hz. In the ac-coupling mode, the influence of the Rogowski coil is amplified by the 1 Hz high-pass filter of the digitizer ac-coupling input stage.

Since, in the voltage channel, the ac-coupling behavior is suppressed by the resistive dividers, the difference between the voltage and current channels is enlarged and different cutoff frequencies are found in the range between 0.3 Hz and 2.5 Hz.

The low-pass filter behavior of the 16.8M-R divider will have an effect on the total energy. However, if we would apply equivalent low-pass filtering on the current channel as well, the suppressed high-frequency voltage components would only be multiplied by lower frequency current components, which will not *a priori* improve the measurement result of the total amount of energy. Furthermore, the expectation is that applying a high-pass filter in the voltage signal to compensate for the input stage of the Rogowski coil would already meet our accuracy requirements for the two wideband dividers and perhaps even for the limited bandwidth divider. Therefore, for the equivalent-filtering method, the implementation will concentrate on the high-pass filters that have a larger impact on the 50 Hz component and, consequently, on the energy calculations.

To simplify the implementation of the method, only the difference between the current and voltage-channel transfer functions is implemented in one of the two channels. A simple first-order high-pass infinite impulse response (IRR) filter was implemented to process the voltage data before calculating the energy. Since IRR filtering is not too computationally intensive, this method was implemented in the data-acquisition software such that the waveform correction and energy calculation is performed real time.

A Butterworth filter was chosen because it is designed to have a frequency response as flat as possible in the passband, which is important for accurate energy calculation. For each combination of coupling setting and voltage divider, the high-pass cutoff frequency f_c is selected such that the phase error between voltage and current at 50 Hz, where most of the energy is concentrated, is minimized. The transfer characteristics of the applied first-order high-pass filter function can be expressed in the complex frequency domain as

$$H(s) = \frac{s}{2\pi f_c + s}. \tag{3}$$

To demonstrate the method, pure sinewave and CL75 voltage and current signals have been measured using the digitizer unit with the Butterworth high-pass filter (3) implemented.

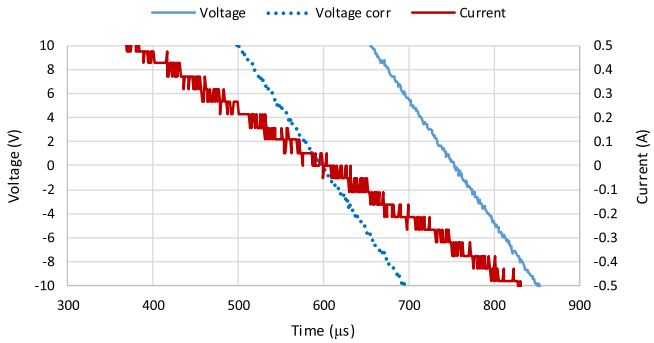

Fig. 6. Equivalent-filter method applied to the same sinusoidal waveform as presented in Figs. 2 and 5. As explained in the text, the cutoff frequency is selected such that the corrected sinusoidal voltage waveform is perfectly synchronized with the current signal. For the CL75 waveform, the equivalent-filter correction has no influence (not shown in the figure).

TABLE I
DESCRIPTION OF WAVEFORMS

Waveform	Power (W)	Power factor	Max. current (A)	Max. dI/dt (A/µs)	Crest factor
PF1	1150	1.00	7.07	0.0022	1.41
PF0.866	996	0.87	7.07	0.0022	1.41
R75	61	0.28	3.66	1.16	3.88
CL75	293	0.19	54.6	2.13	8.19
CL50	329	0.23	51.5	2.05	8.37
WP4	34	0.09	23.8	3.98	13.9
WP9	68	0.18	18.7	3.57	11.2
TK90	380	0.23	50.0	2.50	6.96
TK135	242	0.15	50.0	2.50	6.96
TK165	48	0.03	50.0	2.50	6.96

The measurements presented in Fig. 6 show that proper phase displacement is obtained for the same sinusoidal 50 Hz, 230 V, 5 A waveform, as shown in Fig. 5. The compensated high-frequency distortion of the CL75 signal showed no noticeable changes with respect to the original waveform when using the equivalent-filtering method, just like for the inverse-filtering method.

V. VALIDATION BY ENERGY ERROR DETERMINATION

A. General Approach of Energy Error Determination

Apart from the effect of the correction methods on the waveforms, their effect on energy calculations should be assessed as well. As mentioned in Sections IV-B and IV-C, the inverse-filtering method was used for postprocessing the data recorded using the digitizer unit without further real-time digital signal compensation, while the equivalent-filtering method was implemented as a user-selectable option in the home-built waveform recorder for real-time compensation of the phase mismatch when calculating the active energy. The input stages of the waveform recorder were provided with different voltage dividers, coupling settings, and selections of equivalent filtering.

B. Description of Waveforms

The current and voltage waveforms were generated and measured using the reference testbed with an uncertainty of

0.10%, as already indicated in Section III-A. Artificial waveforms as well as waveforms recorded for real loads applied to a power source were selected. Table I gives an overview of the waveforms used for the specific tests described here and their main parameters. The PF1 waveform, a sinusoidal 230 V, 5 A, 50 Hz signal with unity power factor, was used for calibration purposes. The PF0.866 waveform is the same but with power factor PF = 0.866, i.e., a 30° phase shift between voltage and current.

The recorded waveform representing a resistive heater with a phase-fired dimmer setting of 75% is labeled R75. The earlier mentioned CL75 signal that is shown in detail in Fig. 3 has a 50% dimmed equivalent labeled CL50, which has a sharp current peak centered near the peak of the voltage waveform on top of some rather smooth nonzero content. A commercial water pump with ten different dimmer settings, two of which are labeled WP4 and WP9 in this study, showed a sharply peaked unipolar waveform, in which the dimming operation is performed by simply shifting the current with respect to the voltage. The waveforms, R75, CL75, CL50, WP4, and WP9, are described in more detail in [17].

Furthermore, some artificial waveforms were used, showing a triangular shape with one of the legs showing an extra kink, with the peak value at phase angles of 90°, 135°, and 165° with respect to the voltage signal, labeled TK90, TK135, and TK165, respectively. The latter TK165 waveform is rather extreme in the sense that the current content is concentrated close to the zero crossing of the voltage waveform resulting in a very low power factor, which does not represent a realistic practical situation. This waveform was nevertheless selected to investigate the limits of the measurement capabilities. Since the real load signals have distorted voltages due to the output impedance of the power source, for the latter artificial waveforms, the voltage waveforms were deformed as well, by assuming a resistive grid impedance of 0.8 Ω. In reality, the grid impedance strongly depends on the actual grid topology; a resistive impedance is chosen here as a first attempt to simulate different deformations of the voltage and current channel input filters.

C. Error Measurement Method

The improved phase mismatch compensation methods were compared for their accuracy in energy calculations. The energy readings of the digitizer unit E_{MUT} were compared to the reference-testbed readings E_{REF}

$$\varepsilon_{\mathrm{MUT}} = \frac{E_{\mathrm{MUT}} - E_{\mathrm{REF}}}{E_{\mathrm{REF}}} \times 100\%. \tag{4}$$

The resulting error readings $\varepsilon_{\mathrm{MUT}}$ were obtained when implementing no correction method, a time-shift correction, the inverse-filtering method, and the equivalent-filtering method.

The time-shift correction and the equivalent-filtering method were implemented real time, whereas the recorded waveforms without correction were postprocessed using the inverse-filtering method to calculate the energy and the corresponding error readings. For each combination of coupling setting, voltage divider, and filtering method, the digitizer was recalibrated by adjusting its gain settings to provide zero error reading for the PF1 signal. Similarly, for each combination of coupling setting and voltage divider, the phase angle for the time-shift correction and the high-pass cutoff frequency of the equivalent-filtering method were tuned by matching the phase of the observed voltage and current fundamental-frequency components at 50 Hz. It should be noted that for cases where a large cutoff frequency such as 2 Hz is required, the impact on the measured amplitude at 50 Hz becomes in the order of 0.10%. By adjusting gain settings to account for this amplitude error at 50 Hz, the measured amplitude of higher frequency components will also be affected.

TABLE II

(a) METER ERRORS FOR THE 16.8M-R DIVIDER WITH AC COUPLING. (b) METER ERRORS FOR THE 16.8M-RC DIVIDER WITH AC COUPLING. (c) METER ERRORS FOR THE 1.68M-RC DIVIDER WITH AC COUPLING

(a)

Label	None	Time	Inverse	Equivalent
PF0.866	-2.7 %	0.0 %	0.2 %	0.0 %
R75	8.5 %	0.0 %	-0.5 %	-1.0 %
CL75	0.2 %	10.3 %	0.3 %	-2.9 %
CL50	-2.0 %	7.2 %	0.4 %	-2.3 %
WP4	3.9 %	4.6 %	-1.6 %	-3.2 %
WP9	0.1 %	1.5 %	-0.3 %	-1.1 %
TK90	0.7 %	4.6 %	0.1 %	0.4 %
TK135	6.7 %	7.0 %	-0.3 %	0.6 %
TK165	45.4 %	35.0 %	-1.4 %	1.9 %

(b)

Label	None	Time	Inverse	Equivalent
PF0.866	-2.3 %	0.2 %	0.2 %	0.1 %
R75	7.2 %	-0.6 %	-0.5 %	-0.7 %
CL75	2.4 %	10.6 %	0.0 %	-0.1 %
CL50	0.0 %	7.4 %	0.2 %	0.1 %
WP4	5.2 %	4.0 %	-1.2 %	-0.5 %
WP9	0.5 %	2.2 %	-0.5 %	-0.3 %
TK90	0.3 %	4.7 %	0.1 %	-0.1 %
TK135	5.0 %	7.0 %	-0.4 %	-0.3 %
TK165	33.9 %	34.9 %	-2.7 %	-1.8 %

(c)

Label	None	Time	Inverse	Equivalent
PF0.866	-0.7 %	0.0 %	-0.1 %	0.1 %
R75	1.5 %	-0.5 %	-0.6 %	-0.4 %
CL75	0.6 %	5.6 %	-0.1 %	-0.1 %
CL50	-0.1 %	4.0 %	-0.1 %	0.1 %
WP4	1.1 %	2.7 %	-0.7 %	-0.9 %
WP9	-0.2 %	0.4 %	-0.5 %	-0.3 %
TK90	0.0 %	1.0 %	-0.1 %	0.0 %
TK135	1.3 %	1.4 %	-0.2 %	-0.1 %
TK165	9.0 %	6.8 %	-0.8 %	-1.3 %

D. Error Measurement Results

Measurement errors are calculated using (1) and (4) for four different compensation methods: no correction, the time-shift

TABLE III

(a) METER ERRORS FOR THE 16.8M-R DIVIDER WITH DC COUPLING. (b) METER ERRORS FOR THE 16.8M-RC DIVIDER WITH DC COUPLING. (c) METER ERRORS FOR THE 1.68M-RC DIVIDER WITH DC COUPLING

(a)

Label	None	Time	Inverse	Equivalent
PF0.866	-0.9 %	0.0 %	-0.1 %	-0.1 %
R75	2.6 %	-0.3 %	0.1 %	0.2 %
CL75	-1.9 %	3.5 %	0.2 %	-2.9 %
CL50	-2.1 %	2.6 %	0.2 %	-2.1 %
WP4	0.1 %	1.0 %	0.0 %	-1.4 %
WP9	-0.4 %	0.5 %	0.0 %	-0.9 %
TK90	0.6 %	0.7 %	0.0 %	0.5 %
TK135	2.7 %	1.1 %	0.0 %	0.9 %
TK165	16.5 %	5.0 %	0.1 %	4.4 %

(b)

Label	None	Time	Inverse	Equivalent
PF0.866	-0.4 %	-0.1 %	0.0 %	-0.1 %
R75	0.7 %	-0.4 %	-0.6 %	-0.7 %
CL75	0.5 %	3.7 %	0.1 %	0.0 %
CL50	0.2 %	2.5 %	0.2 %	-0.1 %
WP4	0.3 %	1.0 %	-0.6 %	-1.1 %
WP9	-0.3 %	0.3 %	-0.4 %	-0.4 %
TK90	0.0 %	0.4 %	-0.1 %	-0.1 %
TK135	0.7 %	0.6 %	-0.2 %	-0.1 %
TK165	5.7 %	4.4 %	-0.4 %	-0.7 %

(c)

Label	None	Time	Inverse	Equivalent
PF0.866	-0.5 %	-0.3 %	-0.1 %	-0.1 %
R75	0.7 %	-0.2 %	-0.4 %	0.1 %
CL75	0.3 %	3.2 %	0.0 %	0.1 %
CL50	-0.1 %	2.1 %	0.0 %	0.0 %
WP4	0.2 %	1.1 %	-0.6 %	-0.7 %
WP9	-0.4 %	0.2 %	-0.4 %	-0.3 %
TK90	-0.1 %	0.3 %	0.0 %	0.0 %
TK135	0.7 %	0.7 %	0.0 %	0.1 %
TK165	5.5 %	3.1 %	0.2 %	0.2 %

correction, the inverse-filtering method, and the equivalent-filtering method. The results are presented in Table II(a)–(c) for the three dividers when using the digitizer unit in ac coupling. For all three dividers, the time-shift correction seems to only improve the PF0.866 and R75 signals, where the fundamental current is the dominant component, at a cost of decreased accuracy for other types of distorted signals. For the great majority of the measurements, the inverse-filtering method provides the best results and the equivalent-filtering method provides good improvement as well. The latter two methods both provide very good results for the broadband resistive-and-capacitive dividers 16.8M-RC and 1.68M-RC.

The measurement results for the different compensation methods when using the digitizer unit in dc coupling are presented in Table III(a)–(c) for the three dividers. For the broadband resistive-and-capacitive dividers, apart from the TK165 signal, the results without compensation were quite good already, due to the smaller phase error between the voltage and current channels. The time-shift correction again seems to only improve the PF0.866 and R75 signals, at the cost of decreased accuracy for the other signals. Both the inverse-filtering method and the equivalent-filtering method provide very good results for all dividers.

VI. DISCUSSION

A. Comparison of Compensation Methods

The energy measurements without any correction, as presented in Tables II(a)–(c) and III(a)–(c), show that metering errors can be significant, especially when using the home-built waveform recorder in the ac-coupling mode in combination with the highest impedance voltage dividers 16.8M-R and 16.8M-RC. It should be noted, however, that in many circumstances, it is desirable to nevertheless use ac coupling due to other reasons, like avoiding low-frequency ground loops or overloading integrator circuits with dc offset currents. Furthermore, as expected, using a broadband 1.68M-RC or 16.8M-RC voltage divider provides better uncorrected results compared to the limited-bandwidth 16.8M-R divider.

For each specific combination of digitizer coupling mode and voltage divider used, the tables show the effect of the different filtering compensation methods for each applied waveform. Significant improvement can be obtained when using the two newly introduced compensation methods, whereas for the time-shift method used by many meter manufacturers [10]–[13], the meter accuracy even deteriorates for signals for which the high-frequency content is significant, as the tables show for example for the CL50 and CL75 signals in all test cases. This can be understood from the description and demonstration in Sections II and III, which shows that the time correction improves the synchronization of the 50 Hz component but shifts the higher frequency voltage and current disturbances away from each other. This introduces calculation errors when multiplying the corresponding instantaneous current and voltage values to obtain the energy as in (1).

The inverse-filtering method seems to provide the best measurement results in terms of metering errors for almost all test cases. For most of the waveforms, for all dividers and both coupling settings, most of the reading errors were reduced to below 0.5%, which is well within the accuracy target of 2.0%. This is especially the case for the limited-bandwidth voltage divider, for which Tables II(a) and III(a) show that the uncorrected waveform recorder provides some significant energy-reading errors. Less favorable results are obtained for the WP4 and TK165 waveforms when using ac coupling, for which the maximum obtained errors were -1.6% and -2.7%, respectively. It should be mentioned, however, that all metering errors are expressed in relative terms and the energy content of the two waveforms mentioned is only 34 and 48 W, respectively. Furthermore, as mentioned in Section V-B, the TK165 waveform was chosen only to search for the limits of the measurement capabilities and does not represent a realistic situation. Nevertheless, using the proper hardware, Table II(c) shows that the errors were found to be within 1.0%

for all waveforms investigated. For less-optimized hardware, some further improvement might be obtained when further optimizing the inverse transfer functions. For instance, for the 16.8M-R divider, the magnitudes of the inverse transfer function were set to unity for frequencies above 20 kHz to reduce the noise, which might need further fine-tuning. An obvious disadvantage of this method, however, is that the transfer functions of the voltage and current channels need to be determined, which is not always possible. Furthermore, the method is more computationally intensive than the other methods, which could prevent manufacturers from implementation in their devices.

The equivalent-filtering method shows good results for most test situations as well, although a few more reading errors larger than 1.0% have been observed compared with the inverse-filtering method, especially for the limited bandwidth divider [see Tables II(a) and III(a)]. The equivalent-filtering method could be improved upon by introducing a second digital filter to even better mimic the input filter of the opposing input channel. The fundamental drawback of the method is that only phase displacements are corrected, whereas magnitude errors remain, that is, once energy content is attenuated by the filtering mechanisms of the input stages, it cannot be recovered as in the case of the inverse-filtering method. The major advantage is that it is less computationally intensive such that it can be implemented in electricity meters relatively easy. Furthermore, this method can also be realized using analog filters.

B. Uncertainty Calculations

The uncertainty of the energy reading of the waveform recorder is dependent on the details of the hardware and the specific waveform. When calculating and comparing the uncertainties, we focus on the more common signals that can be expected in real life and therefore do not consider the TK165 waveform, which has an extremely low power factor and can be considered not very realistic. Furthermore, we consider the case of ac coupling and broadband voltage dividers. Under these hypotheses, the total uncertainty is determined by contributions related to: 1) the equipment used to perform the measurements; 2) the method used to compensate for the input stage; and 3) the specific waveform. When calculating the uncertainties, a distinction is made between sinusoidal and nonsinusoidal waveforms, dealing with the latter by considering, for each compensation technique, the largest deviations found with respect to the reference measurements, that is, rather than calculating an uncertainty for each individual waveform, the distorted waveforms are treated all together such that an uncertainty estimate can be provided for all distorted waveforms that fall within our scope of investigation. From our experience, the waveforms investigated here show some of the most deteriorating waveforms, with peak currents up to 55 A and maximum dI/dt up to 4 A/μs, and significant broadband frequency content up to around 50 kHz with crest factors up to 14, providing the largest error readings for electricity meters found so far [7], [8], [17], [18]. The lowest active power investigated was 34 W and the lowest power factor taken into consideration was equal to PF = 0.09, which sets the boundaries of application of the methods. This is well beyond the application ranges of present standards for electricity meter testing [1], [23], [24]. For lower power and lower power factors, the method still works, but probably, the uncertainties will increase.

TABLE IV
EXPANDED UNCERTAINTY OF WAVEFORM RECORDER WITH BROADBAND VOLTAGE DIVIDER FOR DIFFERENT COMPENSATION METHODS

Waveform	None	Time	Inverse	Equivalent
Sinusoidal	3.5 %	0.5 %	0.5 %	0.5 %
Highly-distorted	8.8 %	13.0 %	1.9 %	1.8 %

The uncertainty contributions related to the measurement equipment used are the positioning of the conductors in the Rogowski coil (0.3%, uniform distribution), the accuracy of the voltage dividers (0.5%, normal distribution), the calibration of the digitizer unit (0.10%, normal distribution), and the reference testbed (0.05%, normal distribution). The uncertainty of the application of the inverse-filtering method and the equivalent-filtering method has been estimated by considering Tables II(b) and (c) and III(a) and (b), in which the maximum error for the waveforms except TK165 is 1.2% and 1.1%, respectively. If we consider these numbers as boundaries of uniform probability distributions, this leads to a total expanded uncertainty of 1.9% and 1.8% ($k = 2$, i.e., with a confidence level of about 95% [22]). For some extreme (and less realistic) waveforms with low energy content such as the TK165 signal, the uncertainty will be somewhat larger.

As an example, to show the capabilities of the different compensation methods, a summary of the corresponding expanded uncertainties ($k = 2$ or 95% confidence level) is presented in Table IV when using the broadband voltage dividers, not considering the TK165 signal. The uncertainties were calculated in a similar way as in the previous paragraph, using the maximum errors in Tables II(b) and (c) and III(b) and (c) as boundaries of uniform distributions. For sinusoidal 50 Hz signals, the voltage divider uncertainty is negligible since it is combined with the digitizer calibration. It should be emphasized that the exact numbers in this table depend on the selected hardware configuration. As can be seen in the table, the time-shift correction improves the uncertainty for sinusoidal signals but deteriorates the uncertainty for highly distorted signals, as expected and explained in Section II-A. Both the inverse-filtering method and the equivalent-filtering method show good results for sinusoidal signals and highly distorted signals. The equivalent-filtering method seems slightly better in this case than the inverse-filtering method, but the overall picture from Tables II(a)–(c) and III(a)–(c) is still that the inverse-filtering method provides similar or even slightly better results for almost all waveforms and test cases, especially for the lower bandwidth divider [see Tables II(a) and III(a)].

VII. CONCLUSION

In this article, using a home-built waveform recorder that was modified to operate as static electricity meter, we have

shown that the familiar time-shift correction method to compensate for the difference in input stages of the voltage and current channels is beneficial for sinusoidal signals with little distortion but introduces misalignment of the high-frequency disturbances, and, consequently, miscalculations of the energy and hence metering errors for nonsinusoidal signals. For highly distorted waveforms, these miscalculations can, in fact, increase the reading errors rather than improve the energy readings. Two alternative methods are presented to avoid these errors and to correct the errors introduced by the time-shift method. In the inverse-filtering method, the voltage and current channel inverse transfer functions are implemented in the software to correct for their filtering behavior. The equivalent-filtering method, instead, does not correct for the transfer functions but simply ensures that the voltage and current signals effectively propagate through equivalent input stages by implementing an extra filter in one of the channels such that the instantaneous voltage and current values are properly multiplied.

Validation measurements of metering errors have been performed on a home-built electricity meter to verify and compare the operation of the correction methods for broadband highly distorted waveforms with peak currents up to 55 A, maximum dI/dt of 4 A/μs, significant broadband frequency content up to around 50 kHz with crest factors up to 14, and with the lowest active power of 34 W and power factors as low as PF $=$ 0.03, which covers the most severe distortions found so far and is well beyond the current scope of electricity meter testing standards. For parameters beyond this range of application, the two proposed methods still work, but the uncertainties will increase. The inverse-filtering method was shown to be the most powerful leading to the best measurement results, especially for the lower bandwidth voltage divider. This method is rather computationally intensive, however, which makes it less suitable for simple implementation in inexpensive electricity meters but might be beneficial in high-accuracy power meters or waveform recorders. The equivalent-filtering method showed very good results as well and might be a better candidate for implementation in inexpensive electricity meters or other less-accurate power meters.

Both methods can be applied in static electricity meters as an improved alternative to the commonly used time corrections, ensuring phase alignment at the fundamental frequency without introducing time-shift errors at higher frequencies. Using proper hardware (in specific a broadband and lower resistance voltage divider) in combination with the presented compensation methods, the reading errors of a home-built waveform recorder, modified to operate as an electricity meter, were reduced to below 1.0% using the two presented methods for all signals investigated. This was validated by a testbed having an uncertainty of 0.10%. The final expanded uncertainty of the energy reading is larger due to the imperfectness of auxiliary equipment such as voltage dividers and the limitations of the correction method, but is within the target uncertainty of 2.0% ($k = 2$) for realistic highly distorted waveforms with power factor above PF $=$ 0.09, though it will remain dependent on the waveform details. These results indicate that the adjusted waveform recorder might serve, for instance, as a benchmark meter in case of disputes between energy providers and customers.

ACKNOWLEDGMENT

The research leading to the results described in this article is performed within the project 17NRM02 MeterEMI of the European Metrology Programme for Innovation and Research (EMPIR).

REFERENCES

[1] *Electricity Metering Equipment (A.C.)—Particular Requirements Part 21: Static Meters for Active Energy (Classes 1 and 2)*, Standard IEC 62053-21, 2020.

[2] D. Gallo, C. Landi, N. Pasquino, and N. Polese, "A new methodological approach to quality assurance of energy meters under nonsinusoidal conditions," *IEEE Trans. Instrum. Meas.*, vol. 56, no. 5, pp. 1694–1702, Oct. 2007.

[3] A. Ferrero, M. Faifer, and S. Salicone, "On testing the electronic revenue energy meters," *IEEE Trans. Instrum. Meas.*, vol. 58, no. 9, pp. 3042–3049, Sep. 2009.

[4] E. O. A. Larsson, M. H. J. Bollen, M. G. Wahlberg, C. M. Lundmark, and S. K. Ronnberg, "Measurements of high-frequency (2–150 kHz) distortion in low-voltage networks," *IEEE Trans. Power Del.*, vol. 25, no. 3, pp. 1749–1757, Jul. 2010.

[5] *Electricity Metering Equipment (A.C.)—Severity Levels, Immunity Requirements and Test Methods for Conducted Disturbances in the Frequency Range 2 kHz–150 kHz*, Standard CLC TR 50579, 2012.

[6] *Electromagnetic Compatibility (EMC)—Part 4-19: Testing and Measurement Techniques—Test for Immunity to Conducted, Differential Mode Disturbances and Signalling in the Frequency Range 2 kHz to 150 kHz at A.C. Power Ports*, Standard CLC TR 50579, 2014.

[7] F. Leferink, C. Keyer, and A. Melentjev, "Static energy meter errors caused by conducted electromagnetic interference," *IEEE Electromagn. Compat. Mag.*, vol. 5, no. 4, pp. 49–55, 4th Quart., 2016.

[8] G. Rietveld, D. Hoogenboom, and M. Acanski, "Conducted EMI causing error readings of static electricity meters," in *Proc. Conf. Precis. Electromagn. Meas.*, Paris, France, Jul. 2018, pp. 1–2.

[9] Z. Marais, H. E. van den Brom, G. Rietveld, R. van Leeuwen, D. Hoogenboom, and J. Rens, "Sensitivity of static energy meter reading errors to changes in non-sinusoidal load conditions," in *Proc. Int. Symp. Electromagn. Compat. EMC EUROPE*, Barcelona, Spain, Sep. 2019, pp. 202–207.

[10] S. English and D. Smith, "A power meter reference design based on the ADE7756," Analog Devices, Norwood, MA, USA, Appl. Note AN-564, 2001.

[11] *MCP3909 3-Phase Energy Meter Reference Design Using PIC18F2520*, User's Guide, Microchip Technol., Chandler, AZ, USA, 2007.

[12] K. Tang, "Reference design for an energy meter using the MAXQ3180/MAXQ3183 AFEs," Maxim Integr. Products, San Jose, CA, USA, Appl. Note 4663, Oct. 2010.

[13] M. Mesganaw and S. Underwood, "Implementation of a low-cost three-phase electronic watt-hour meter using the MSP430F67641," Texas Instrum., Dallas, TX, USA, Appl. Rep. SLAA621C, Aug. 2015.

[14] *Voltage Characteristics of Electricity Supplied by Public Electricity Networks*, Standard EN 50160, 2010.

[15] M. Mienkina, "Filter-based algorithm for metering applications," NXP Semicond., Eindhoven, The Netherlands, Appl. Note AN4265, Apr. 2016.

[16] H. E. van den Brom, Z. Marais, D. Hoogenboom, R. van Leeuwen, and G. Rietveld, "A testbed for static electricity meter testing with conducted EMI," in *Proc. Int. Symp. Electromagn. Compat. EMC EUROPE*, Barcelona, Spain, Sep. 2019, pp. 603–608.

[17] R. van Leeuwen, H. van den Brom, D. Hoogenboom, G. Kok, and G. Rietveld, "Current waveforms of household appliances for advanced meter testing," in *Proc. IEEE 10th Int. Workshop Appl. Meas. Power Syst. (AMPS)*, Aachen, Germany, Sep. 2019, pp. 1–6.

[18] B. T. Have, T. Hartman, N. Moonen, C. Keyer, and F. Leferink, "Faulty readings of static energy meters caused by conducted electromagnetic interference from a water pump," *Renew. Energy Power Qual. J.*, vol. 17, pp. 15–19, Jul. 2019.

[19] T. Hartman, M. Pous, M. A. Azpurua, F. Silva, and F. Leferink, "On-site waveform characterization at static meters loaded with electrical vehicle chargers," in *Proc. Int. Symp. Electromagn. Compat. (EMC EUROPE)*, Barcelona, Spain, Sep. 2019, pp. 191–196.

[20] K. Lind, T. Sørsdal, and H. Slinde, "Design, modeling, and verification of high-performance AC–DC current shunts from inexpensive components," *IEEE Trans. Instrum. Meas.*, vol. 57, no. 1, pp. 176–181, Jan. 2008.
[21] J. O. Smith, *Mathematics of the Discrete Fourier Transform (DFT) With Audio Applications*, 2nd ed. W3K Publishing, 2007. [Online]. Available: http://ccrma.stanford.edu/~jos/mdft/
[22] *Guide to the Expression Of Uncertainty in Measurement*, Standard JCGM 100, 2008.
[23] *Electricity Metering Equipment (A.C.)–Particular Requirements—Part 22: Static Meters for Active Energy (Classes 0,2 S and 0,5 S)*, Standard IEC 62053-22, 2020.
[24] *Electricity Metering Equipment (A.C.) Part 3: Particular Requirements–Static Meters for Active Energy (Class Indexes A, B and C)*, Standard EN 50470-3, 2006.

Zander Marais was born in Vereeniging, South Africa, in 1994. He received the M.Eng. degree in electrical and electronic engineering from North West University, Potchefstroom, South Africa, in 2019.

From 2017 to 2018, he was part of the NWU Solar Team that competed in the 2017 Sasol Solar Challenge and the 2018 Bridgestone World Solar Challenge. He was involved in designing the energy management system and electrical systems for two solar-powered electric vehicles that competed in these races. In 2019, he joined VSL B.V., Delft, The Netherlands, where he started working on a test setup for characterizing static electricity meters under distorted load conditions. He is also involved in ac/dc transfer and impedance measurements. His research interests are energy measurement systems, harmonics, power quality, electromagnetic compatibility, and sampling systems.

Helko E. van den Brom (Senior Member, IEEE) was born in Utrecht, The Netherlands, in 1971. He received the M.Sc. degree in theoretical solid-state physics from Utrecht University, Utrecht, in 1995, and the Ph.D. degree in experimental solid-state physics from Leiden University, Leiden, The Netherlands, in 2000.

In 2000, he joined VSL B.V., Delft, The Netherlands, where he started working on the development of Josephson and SET-based electrical quantum standards. At present, as a principal scientist, his current research interests are in power quality, electricity meters, current and voltage transducers, and sampling systems.

Dr. van den Brom is a member of the Dutch Physical Society (NNV), a Technical Assessor for the Dutch Accreditation Council (RvA), and a Contact Person for VSL in the Technical Committee of Electricity and Magnetism (TCEM) of the European Association of National Metrology Institutes (EURAMET). He was a recipient of the Best Ph.D. Paper Award of the *Dutch Journal of Physics* (NTvN) in 2000. He is also an Associate Editor of the IEEE TRANSACTIONS ON INSTRUMENTATION AND MEASUREMENT.

Gertjan (G. J. P.) Kok was born in Leiderdorp, The Netherlands, in 1981. He received the M.Sc. degree in applied mathematics and general engineering from TU Wien, Vienna, Austria, and the École Centrale Paris, Paris, France, respectively, in 2005, after having followed the international double degree program TIME.

In 2008, he joined VSL B.V., Delft, The Netherlands, as a Research Scientist. He is specialized in mathematical modeling, data analysis, and uncertainty calculations that he performs for a wide range of applications, ranging from electrical to fluid flow and length measurements. One of his newer research interests relates to performing metrological sound data analyses in the context of Industry 4.0 and involving machine learning algorithms.

Marijn G. A. van Veghel was born in 's-Hertogenbosch, The Netherlands, in 1976. He received the M.Sc. degree (*cum laude*) and the Ph.D. degree in physics from Utrecht University, Utrecht, The Netherlands, in 1999 and 2004, respectively.

In 2005, he joined VSL B.V., Delft, The Netherlands, where he worked as a Research Scientist in dimensional metrology and a consultant in metrology for high-tech systems. Since 2017, he has been the Project Manager for the Electricity group and in that capacity manages all research projects and customer projects. His current project portfolio includes a number of projects on smart metering and power quality. He also teaches a course on uncertainty estimation.